Available online at www.sciencedirect.com
SCIENCE DIRECT®
ELSEVIER
International Journal of Solids and Structures 43 (2006) 1331–1356
INTERNATIONAL JOURNAL OF SOLIDS and STRUCTURES
www.elsevier.com/locate/ijsolstr

Mechanics of the rate-dependent elastic–plastic deformation of glassy polymers from low to high strain rates

A.D. Mulliken, M.C. Boyce *

Department of Mechanical Engineering, Institute for Soldier Nanotechnologies, Massachusetts Institute of Technology, Room 1-304, 77 Massachusetts Avenue, Cambridge, MA 02139, USA

Received 15 November 2004; received in revised form 16 April 2005
Available online 8 June 2005

Abstract

A combined experimental and analytical investigation has been performed to understand the mechanical behavior of two amorphous polymers—polycarbonate and poly(methyl methacrylate)—at strain rates ranging from 10^{-4} to 10^{4} s^{-1}. This range in strain rates was achieved in uniaxial tension and compression tests using a dynamic mechanical analyzer (DMA), a servo-hydraulic testing machine, and an aluminum split-Hopkinson pressure bar. DMA tension tests were used to characterize the viscoelastic behavior of these materials, with focus on the rate-dependent shift of material transition temperatures. Uniaxial compression tests on the servo-hydraulic machine (10^{-4} to 1 s^{-1}) and the split-Hopkinson pressure bar (10^{3} to 10^{4} s^{-1}) were used to characterize the rate-dependent yield and post-yield behavior. Both materials were observed to exhibit increased rate sensitivity of yield under the same strain rate/temperature conditions as the β-transition of the viscoelastic behavior. A physically based constitutive model for large strain deformation of thermoplastics was then extended to encompass high-rate conditions. The model accounts for the contributions of different molecular motions which become operational and important in different frequency regimes. The new features enable the model to not only capture the transition in the yield behavior, but also accurately predict the post-yield, large strain behavior over a wide range of temperatures and strain rates.

Keywords: Polymer; High-rate; Split-Hopkinson; Constitutive behavior

1. Background

Amorphous polymers have been used extensively as the structural material of engineering components that are designed to resist impact, ranging from bus windows and eyeglasses to helmets and body armor.

* Corresponding author. Tel.: +1 617 253 2342; fax: +1 617 258 8742.
E-mail address: mcboyce@mit.edu (M.C. Boyce).

0020-7683/$ - see front matter © 2005 Elsevier Ltd. All rights reserved.
doi:10.1016/j.ijsolstr.2005.04.016

The choice of polymeric materials for these applications has been made appealing by their relative low density, as well as the transparency that is characteristic of amorphous homopolymers. The rate-dependence of the elastic, plastic and failure behavior of polymers is well-known; however, the behavior under very high rates of deformation is still not well understood. It was the goal of this study to develop such an understanding for amorphous polymers, from molecular mechanisms of deformation resistance up to the elastic–viscoplastic stress–strain response, and to use this understanding in the development of a constitutive model that is accurate at all deformation rates.

Fig. 1 shows the yield strength of poly(methyl methacrylate) (PMMA) as a function of both temperature and strain rate, as recorded by Roetling (1965b). This experimental data indicates the existence of a significant transition in the nature of the rate dependence of the material yield behavior. Beyond a transition threshold, the material exhibits an increased sensitivity to strain rate. The transition threshold is determined by both temperature and strain rate. This same phenomenon has been observed in the yield behavior of a variety of amorphous polymers: polycarbonate (PC) (Bauwens-Crowet et al., 1972; Rietsch and Bouette, 1990; Moy et al., 2003), polyvinyl chloride (PVC) (Bauwens et al., 1969; Walley and Field, 1994), poly(ethyl methacrylate) (PEMA) (Roetling, 1965a), and amorphous polyethylene terephthalate (PET) (Foot et al., 1987). The transition threshold, as well as the degree of strain rate sensitivity before and after the transition, is unique to the particular polymer.

Although many theories have emerged to address polymer plasticity, only the Ree–Eyring theory provides an analytical model that is capable of capturing polymer yield behavior across such a transition. The Ree–Eyring theory (Ree and Eyring, 1955) is a modification of the general Eyring theory (Eyring, 1936) for rate-activated processes and allows for multiple rate-activated processes acting in tandem to control the flow of a material. When the Ree–Eyring theory is applied to polymer plasticity, it is assumed that these "processes" are related to specific degrees of freedom of the polymer chains. Thus, under the Ree–Eyring theory, the transition observed in the yield behavior is explained in terms of molecular-level motions. When a particular degree of freedom of the polymer chain suddenly becomes restricted at low temperature and/or high strain rate, the corresponding process begins to contribute to the overall material deformation resistance. Roetling (1965a,b), Bauwens et al. (1969), and Bauwens-Crowet et al. (1969) were the first to capture a transition in polymer yield behavior by applying a two-process Ree–Eyring yield model to data obtained under quasi-static loading conditions over a wide range of temperatures.

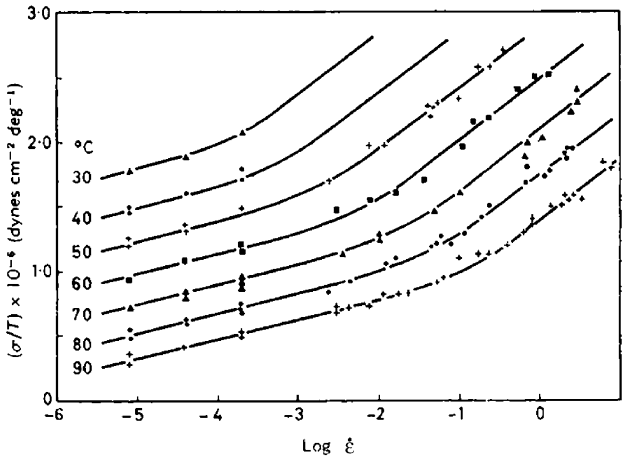

Fig. 1. PMMA yield strength as a function of temperature and strain rate. Reprinted from Roetling (1965b) with permission from Elsevier.

This theory, connecting molecular mechanisms of deformation resistance with macroscopic mechanical behavior, was furthered by Bauwens (1972). Bauwens hypothesized a correlation between the observed transition in material yield behavior with the secondary β-transition of the viscoelastic behavior. He argued that both transitions are governed by the same molecular motions, using measured activation energy values to corroborate his theory. He then built a modified version of the Ree–Eyring yield model, based on viscoelastic loss tangent measurements, that was able to more accurately capture the distributed nature of the yield transition. Over the past three decades, the experimental and analytical work of other researchers has reinforced the ideas of Bauwens and his contemporaries. Split-Hopkinson bar testing has been employed to study the yield and post-yield behavior of polymers at very high strain rates ($>1000\ s^{-1}$) (Kolsky, 1949; Rietsch and Bouette, 1990; Walley and Field, 1994; Moy et al., 2003; Cady et al., 2003; Swallowe and Lee, 2003). The two-process Ree–Eyring yield model has been used extensively to capture material yield behavior over very large ranges in temperature and strain rate (Haussy et al., 1980; Foot et al., 1987; Steer and Rietsch, 1988; Rietsch and Bouette, 1990), where calculated activation energy values have confirmed Bauwens' hypothesis concerning the connection between viscoelastic and yield behavior transitions (Foot et al., 1987).

Through nuclear magnetic resonance (NMR), dielectric measurements, and comparison of the activation and relaxation characteristics of polymers with similar structures, researchers have attempted to identify specific intramolecular motions in association with the β-transitions of different amorphous polymers. Significant discussion on this topic is given by Hutchinson (1997), including a thorough summary of past findings, both complementary and contradictory. Traditionally, the β-transition of PC has been attributed to the restriction of main-chain phenyl group rotations; for PMMA, the β-transition is attributed to the restriction of ester side group rotations. More recently, however, it has been suggested that cooperative intermolecular motions are also involved in these secondary processes (Floudas et al., 1993; Diaz-Calleja et al., 1994; Schartel and Wendorff, 1995). For the purposes of this study, the most significant result is that there does exist some secondary molecular motion, distinct from molecular processes of the α-transition, which has an independent contribution to the macroscopic rate dependence of these materials.

The combined experimental and analytical research program of this study was developed in consideration of the broad base of knowledge and theory that has been established in the literature. On the experimental side, investigation of viscoelastic behavior was chosen as one focal point, in order to gain more fundamental understanding of the material transitions, and to further the linkages between material viscoelastic, yield, and stress–strain behavior. The effects of these transitions on yield and post-yield behavior over a wide range in strain rates, extending up to $1000\ s^{-1}$, was then experimentally explored in large strain compression testing. On the analytical side, the concept of decomposing material resistance to elastic deformation and to initial yield into contributions from two different molecular processes proved central to the analysis and modeling techniques introduced here.

2. Experiments

2.1. Materials

Two amorphous polymers were chosen for investigation in this study: Lexan® polycarbonate manufactured by GE Plastics, and Plexiglas® G poly(methyl methacrylate), manufactured by AtoHaas. All specimens were machined directly from sheet stock and stored in a dessicator cabinet for 3–5 days prior to testing to eliminate any variability in the data caused by changing humidity levels. The Plexiglas G PMMA sheet is produced through a traditional cell cast method, and thus no molecular chain orientation exists in the as-cast sheet. The PC sheet, on the other hand, is produced through an extrusion process, and will exhibit very slight chain orientation in the extrusion direction. While this orientation may significantly affect

the accessibility of various local failure modes in certain loading situations, it has little to no effect on the viscoelastic, yield and post-yield behavior during uniaxial compression. This assertion was verified through post-test analysis of the deformed compression specimens, which were found to be perfectly circular in cross-section.

2.2. Dynamic mechanical analysis

Dynamic mechanical analysis (DMA) testing was performed on a TA Instruments Q800 Dynamic Mechanical Analyzer. Rectangular PC and PMMA specimens were machined from sheet stock approximately 1.6 mm thick; final specimens had approximate dimensions of 20 mm × 3 mm × 1.6 mm. The specimens were loaded in the DMA with a tensile pre-load (0.01 N); displacement control mode was used to oscillate about the pre-strain level such that total strain levels never exceeded 0.1% at temperatures below T_g. Materials were first tested over the entire temperature range of the DMA instrument—from −140 °C to 180 °C—at a frequency of 1 Hz. The storage modulus and loss modulus were measured as a function of temperature, and the corresponding loss tangent was calculated. In this manner, a storage modulus ''reference curve'' was established for each material, and approximate temperature locations of significant material transitions could be determined. The two materials were then tested at frequencies of 1 Hz, 10 Hz, and 100 Hz, over small ranges in temperature around the identified material transitions. The particular frequencies of these tests corresponded to strain rates over the range $1.9 \times 10^{-3}\ s^{-1}$ to $3.2 \times 10^{-1}\ s^{-1}$, depending on the exact specimen gage length and displacement amplitude prescribed.[1] Again, storage modulus and loss modulus information was recorded, and corresponding loss tangent calculations were made.

2.3. Compression testing

Uniaxial compression tests were carried out on PC and PMMA over seven decades of strain rate: $10^{-4}\ s^{-1}$ to approximately $6000\ s^{-1}$. Uniaxial compression was selected as the deformation mode because it dictates a homogeneous stress and deformation state to large strains, making interpretation of the data straightforward. Low to moderate rate testing ($10^{-4}\ s^{-1}$ to $1\ s^{-1}$) was conducted on an Instron servo-hydraulic testing machine. A specially designed feedback loop between the extensometer (which locally measures the current height of the specimen) and the actuator was used to ensure a constant true strain rate over the duration of the tests. Thin Teflon sheets were placed between the Instron platens and specimen surfaces; WD-40 lubricant was used between the Teflon sheets and platens. The lower platen was fit with a spherical seat, to compensate for any small misalignment. All specimens were of right circular cylinder geometry, with diameter of 12.7 mm and length of 6.35 mm. Specimens were machined down from sheet stock of thickness greater than 6.35 mm, with a parallel-face tolerance of less than three one-hundredths of a millimeter. This particular length-to-diameter ratio (1:2) was chosen in order to be consistent with the geometry of the high-rate specimens.

High strain rate testing ($800\ s^{-1}$ to $6000\ s^{-1}$) was performed on a compressive split-Hopkinson bar test apparatus designed in cooperation with and built by Physics Applications, Inc. of Dayton, Ohio. This

[1] The test frequency is converted to a strain rate by examining one-quarter of a cycle in the sinusoidal load program. The time duration of this quarter cycle is known from the test frequency, and the strain amplitude achieved during this time can be calculated from the prescribed displacement amplitude and the known specimen gage length. The increase in strain over this time is approximated to be linear, and thus an average strain rate can be calculated:

$$\dot{\epsilon} = \frac{\text{strain}}{\text{time}} = \frac{\frac{d_0}{l_g}}{\frac{1}{4}\frac{1}{\omega}} \tag{1}$$

where d_0 is the displacement amplitude and l_g is the specimen gage length.

apparatus employs solid aluminum pressure bars, both with a length of approximately 2.3 m and a diameter of 19.05 mm. The theory of split-Hopkinson bar testing has been well-documented; see for instance Davies (1948), Kolsky (1949), or Gray (2000). Recently, issues unique to testing low-impedance, low yield strength materials such as amorphous polymers have been a topic of research for several investigators; this line of work is summarized by Gray and Blumenthal (2000).

Specimens for split-Hopkinson bar testing were also of right circular cylinder geometry, with a diameter of 5.08 mm and a length of 2.54 mm. Previous work has suggested that length-to-diameter ratios of 1:2 or less are necessary in the testing of low-impedance materials on these test systems, in order to minimize wave attenuation in the strain gage signals (Gray et al., 1997; Chen et al., 1999). Also, a length-to-diameter ratio of 1:2 has been shown to be optimal in negating the effects of radial and longitudinal inertia in the specimen (Davies and Hunter, 1963). All specimens were lubricated with a thin layer of petroleum jelly on both faces, and little to no barreling was ever observed. Dynamic equilibrium was achieved before yield in all tests, due to the short specimen lengths. Since DMA testing was used to characterize the rate-dependent elastic moduli, the pre-yield data at high rates was not of consequence and therefore pulse-shaping was unnecessary.

3. Results and analysis

3.1. Dynamic mechanical analysis

Representative storage modulus and loss modulus curves taken at 1 Hz for PC and PMMA are plotted in Figs. 2 and 3, respectively. In both storage modulus curves, there is clear evidence of a glass (α) transition, through which the storage modulus drops off by three orders of magnitude. In the case of PC (Fig. 2), this transition is centered around 150 °C; for PMMA (Fig. 3), it is centered around 115 °C. As expected, the loss modulus curves exhibit a relative maximum in the region of these glass transitions. For both materials, the α-transition is associated with restricted rotations and translations of the polymer main chains.

The loss modulus curves of Figs. 2 and 3 may also act to identify the temperature location of the secondary (β) viscoelastic transitions of PC and PMMA. In the PC curve (Fig. 2), there is a β-peak located at approximately −80 °C—far enough away from the α-peak that the corresponding effect on the storage

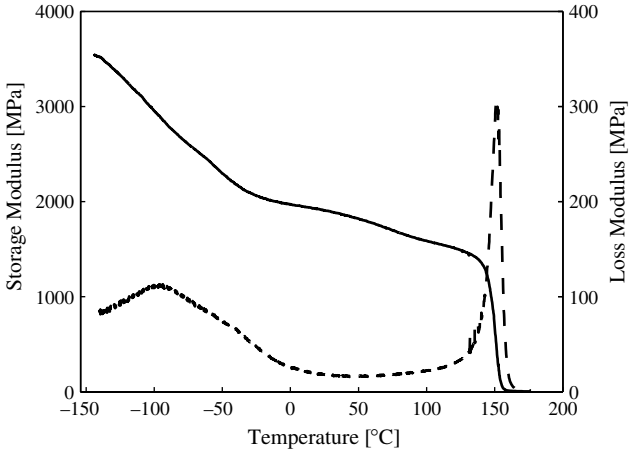

Fig. 2. PC storage modulus (solid line) and loss modulus (dashed line) as a function of temperature at $3.2 \times 10^{-3}\ s^{-1}$ (1 Hz). The loss modulus peaks centered at −95 °C and 150 °C correspond to the β and α transitions, respectively.

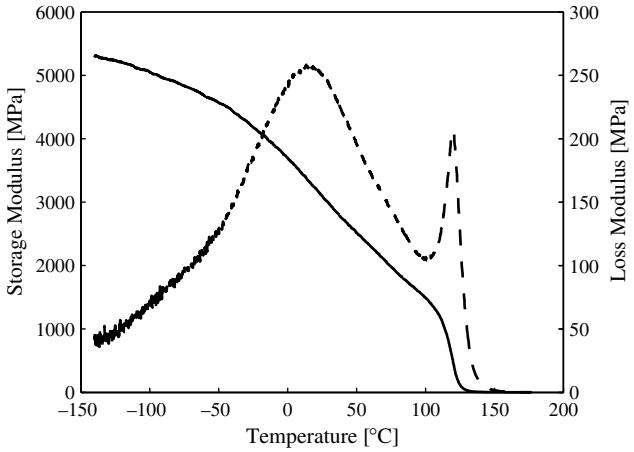

Fig. 3. PMMA storage modulus (solid line) and loss modulus (dashed line) as a function of temperature at $2.1 \times 10^{-3}\ s^{-1}$ (1 Hz). The loss modulus peaks centered at 15 °C and 115 °C correspond to the β and α transitions, respectively.

modulus curve is clear. The storage modulus drops from ~3 GPa at −100 °C to ~2 GPa at −25 °C and then to ~1.7 GPa at 100 °C. For PC, the β-transition is taken to be correlated with the molecular mobility of main-chain phenyl groups.

In the case of PMMA (Fig. 3), the large β-peak overlaps the α-peak a considerable amount at this frequency, and thus only one combined effect is seen in the storage modulus reference curve. The storage modulus drops from ~5 GPa at −100 °C to ~4 GPa at −25 °C and then to ~1.5 GPa at 100 °C. The PMMA β-transition, centered at 15 °C, is correlated with the mobility of the ester side groups with respect to the main chain.

Further DMA testing was conducted in order to determine the rate-dependent shifts of the transition locations. Using the locations identified in Figs. 2 and 3, small ranges of temperature in the region of the α and β transitions were examined at 1 Hz ($\sim 10^{-3}\ s^{-1}$), 10 Hz ($\sim 10^{-2}\ s^{-1}$), and 100 Hz ($\sim 10^{-1}\ s^{-1}$).

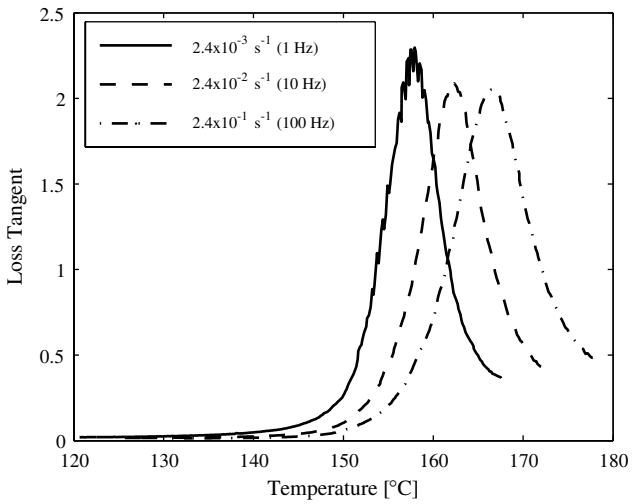

Fig. 4. PC loss tangent ($\tan\delta$) as a function of temperature and strain rate in the region of the α-transition.

Table 1
Shift of PC and PMMA viscoelastic transitions with strain rate

	Shift of α-transition [°C/decade strain rate]	Shift of β-transition [°C/decade strain rate]
PC	4.7	15.3
PMMA	11.1	25.2

In Fig. 4, representative PC loss tangent curves in the region of the α-transition are plotted as a function of temperature and strain rate. The glass (α) transition is observed to shift to higher temperatures with increasing strain rate. By tracing the precise temperature location of the α-peak with increasing strain rate, the shift factor was quantified: the PC glass transition was found to shift approximately 4.7 °C per decade increase in strain rate. An identical procedure was used to quantify the rate-dependent shifts of the α and β transitions of PC and PMMA—the results are summarized in Table 1. In general, the temperature locations of the β transitions are observed to be much more sensitive to changes in strain rate.

In order to predict the elastic behavior at all strain rates and temperatures, the DMA data over the tested frequency and temperature conditions is utilized together with a novel time-temperature shift that specifically takes into account the different rate dependencies of the α and β transitions. In particular, this approach enables accurate characterization of the rate-dependent elastic behavior at the high strain rates ($\sim$1000 s^{-1}) experienced during ballistic impact events.

Analytical expressions for the elastic moduli of PC and PMMA are developed by first decomposing the storage modulus reference curves of Figs. 2 and 3 into their respective α and β components. For the case of PC, the structure of the storage modulus reference curve lends itself well to decomposition: as the curve is traced with decreasing temperature, a significant upturn appears at approximately −25 °C. Based on the loss modulus measurements, this upturn is observed to correlate with the onset of the restriction of the β-process. Following this analysis, the PC storage modulus reference curve was separated into an α- and a β-component, as shown in Fig. 5. These components were then taken to shift with strain rate by the amounts determined via experimental examination of the transition locations, summarized in Table 1. The entire modulus curve could then be reconstructed for any particular strain rate by first shifting the components of the reference curve by the appropriate amounts, and then summing the components at every temperature.

This decompose/shift/reconstruct (DSR) method enables the prediction of the elastic modulus of PC and PMMA at temperatures and strain rates well beyond the capabilities of the DMA instrument. Fig. 6 shows the DSR model prediction of the PC elastic modulus curve at five different strain rates, ranging from 10^{-4} s^{-1} to 10^{4} s^{-1}. The curve not only shifts to the right (increased temperatures) with increasing strain rate, but it also changes shape due to the different shift factors of the α and β components of the curve.[2]

Perhaps more significantly, this DSR method can also be used to predict at what strain rate we would expect to observe a significant transition in material behavior. Assuming that this significant material transition—most often observed in the yield behavior of the polymer—is brought on by the restriction of the same molecular motion associated with the β-transition of the viscoelastic behavior, we may look to the shifting β-transition in Fig. 6 to predict the transition strain rate. Again, this β-transition is identified by the upturn in the storage modulus curve. At strain rates of about 1 s^{-1} and below, the upturn has not yet shifted past room temperature (vertical dashed line)—phenyl group rotations are not yet restricted, and the β contribution to the overall elastic modulus is negligible. However, as the strain rate is increased to 100 s^{-1}, the transition shifts past room temperature and the β contribution rapidly becomes more significant with increasing strain rate. Since the same basic mechanisms which govern elasticity in amorphous

[2] Note that linear viscoelastic theory can be used to express this behavior in terms of relaxation moduli and/or creep compliances as a function of time and temperature.

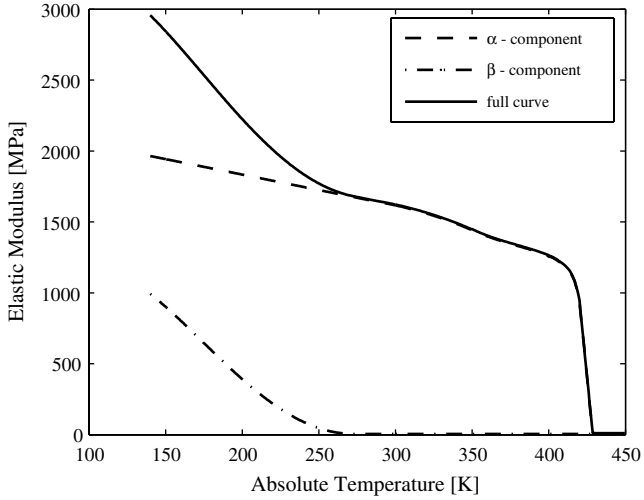

Fig. 5. PC elastic modulus curve at $3.2 \times 10^{-3}\ s^{-1}$ decomposed into α and β components. Curves have been generated from polynomial fits of the split data.

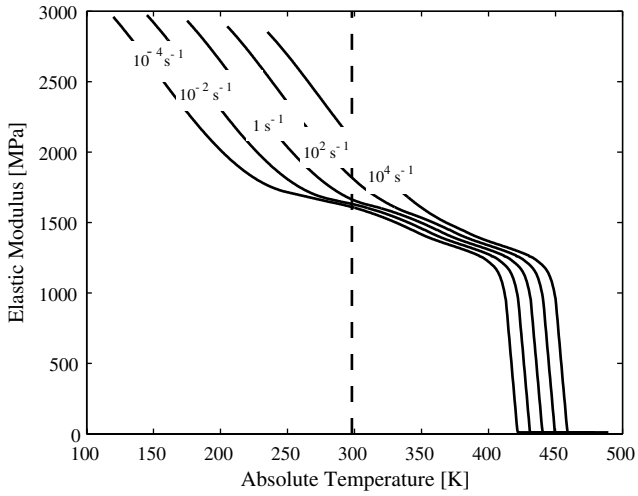

Fig. 6. Model prediction of the PC elastic modulus curve at five strain rates: $10^{-4}\ s^{-1}$ to $10^{4}\ s^{-1}$. The vertical dashed line represents room temperature (298 K).

polymers also govern yield and plasticity, we would expect to observe a transition in the room temperature yield behavior of PC at a similar strain rate—about $100\ s^{-1}$.

Application of the DSR method to the PMMA data was not as straightforward as it was in the case of PC, mainly because of the interaction between the α and β processes across almost every temperature at the reference strain rate. A suitable decomposition of the storage modulus data (Fig. 7) was developed not only from the PMMA storage and loss modulus curves, but also from the methods which best suited the PC decomposition. Combining this analytical decomposition with the experimentally-derived shift factors for the α and β processes, again it was possible to predict at what strain rate we would expect to see a significant transition in the PMMA yield behavior at room temperature. Fig. 8 shows the PMMA elastic

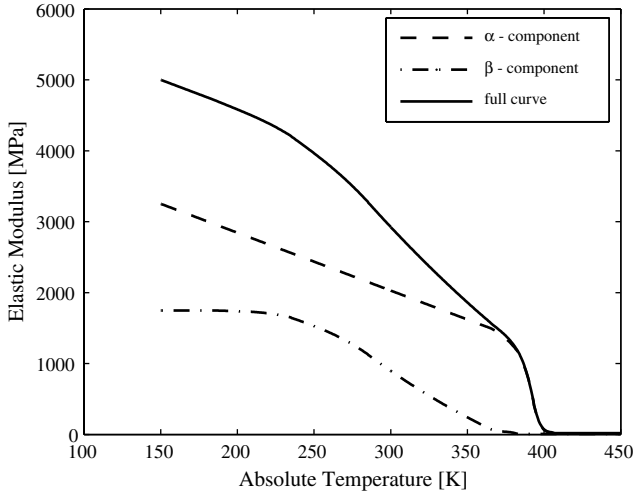

Fig. 7. PMMA elastic modulus curve at $2.1 \times 10^{-3}\ s^{-1}$ decomposed into α and β components. Curves have been generated from polynomial fits of the split data.

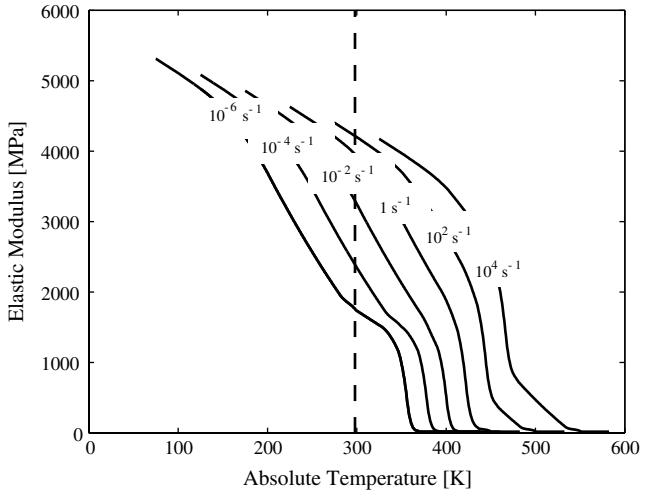

Fig. 8. Model prediction of the PMMA elastic modulus curve at six strain rates: $10^{-6}\ s^{-1}$ to $10^{4}\ s^{-1}$. The vertical dashed line represents room temperature (298 K).

modulus at six different strain rates, as predicted by the DSR model, along with a vertical dashed line representing room temperature. Based on the curves of this figure, the PMMA transition is expected to occur at a strain rate between $10^{-5}\ s^{-1}$ and $10^{-4}\ s^{-1}$.

3.2. Compression testing

During low to moderate rate compression testing on the servo-hydraulic instrument, both PC and PMMA specimens deformed in a ductile manner up to a true strain of 0.80, corresponding to a deformed

height ratio $h/h_0 = 0.45$. The homogeneous nature of the deformation was confirmed via post-mortem analysis of the test specimens; little to no barreling was observed in either the PC or PMMA.

In the case of high-rate testing, the PC specimens deformed in a ductile manner over the tested strain rates, ranging from 1200 s^{-1} to 4000 s^{-1} (true strain rate at yield). In the PMMA tests, brittle failure of the specimens occurred prior to yield at strain rates above 1400 s^{-1}. At rates lower than 1400 s^{-1}, yield and post-yield deformation were observed prior to a brittle failure. In both materials, true strain rates were found to vary over the duration of the tests. However, despite the absence of pulse-shaping techniques, the strain rate varied no more than 25% for both PC and PMMA. Fig. 9 shows representative true strain rate histories, along with the corresponding true stress–true strain curves, for tests on PC and PMMA where the greatest variation in strain rate was observed.

The results of all uniaxial compression testing of PC are summarized in Figs. 10 and 11. Fig. 10 provides a comparison of representative high-rate true stress–true strain curves (1350 s^{-1} and 5050 s^{-1}) with

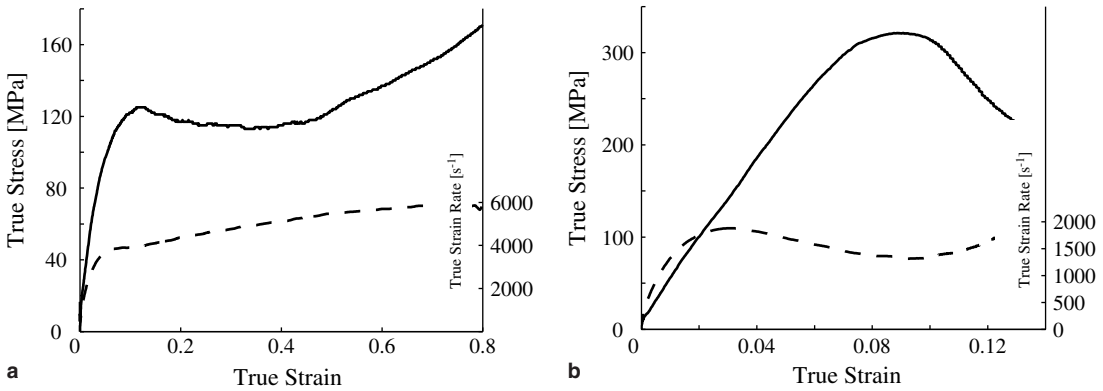

Fig. 9. True stress–true strain behavior and corresponding strain rate histories (a) PC, ~5050 s^{-1} and (b) PMMA, ~1400 s^{-1}.

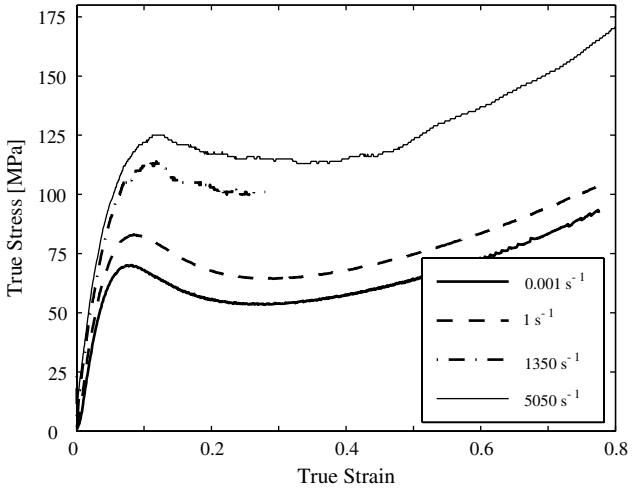

Fig. 10. Representative curves of PC true stress–true strain behavior in uniaxial compression at four low, moderate, and high rates. Reported high strain rates are averages over the duration of the tests.

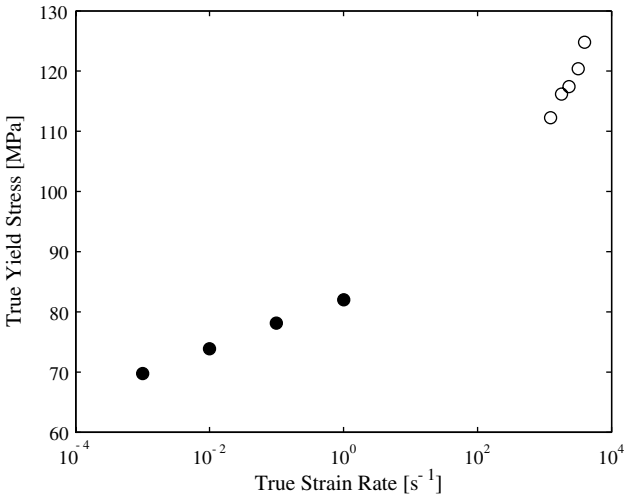

Fig. 11. PC true yield stress as a function of true strain rate (logarithmic scale)—low to high strain rates. Each data point represents an average of at least two tests on either the servo-hydraulic Instron (●) or the compressive split-Hopkinson bar (○).

representative low to moderate rate curves (10^{-3} and 1 s^{-1}). All of the curves indicate the expected features of material response to large-strain uniaxial deformation: initial linear elasticity, non-linear transition to global yield, followed by strain softening and subsequent strain hardening. It is observed that, in general, the relative significance of each of these features remains constant through this range of strain rates.

Fig. 11 shows the PC yield strength as a function of strain rate across all of the tested strain rates. Within the low to moderate rate regime, the yield stress is found to increase linearly with the logarithm of strain rate, indicating that yield behavior in this regime could be accurately explained and/or predicted in terms of a single activated process. This finding is in agreement with the work of Bauwens et al. (1969), Walley and Field (1994), and Moy et al. (2003), among others. In the high-rate regime, again the yield strength is found to increase in an approximately linear fashion with the logarithm of strain rate. However, the slope of the data line is much greater in this high-rate regime. It is clear that PC undergoes a significant material transition as the strain rate is increased beyond a certain critical level, located between the test capabilities of the servo-hydraulic machine and the test capabilities of the split-Hopkinson bar apparatus. The yield data generated here indicates that the transition is centered around a strain rate of approximately 150 s^{-1}. This transition strain rate is consistent with the DSR model prediction of the transition in the rate-dependent mechanical behavior.

The results of all uniaxial compression testing of PMMA are summarized in Figs. 12 and 13. Fig. 12 shows representative true stress–true strain curves for PMMA across all of the tested strain rates. In this case, the characteristic shape of the stress–strain curve is not the same at all rates. At moderate strain rates, the PMMA exhibits significantly more post-yield softening than at low strain rates, as also seen in the work of Arruda et al. (1995). The increased softening effect has been shown to be due to non-isothermal test conditions as the strain rate is increased. A fraction of the plastic work is converted to heat, and thus the polymer experiences thermal softening with increased plastic straining when the strain rate is sufficiently high such that all of the heat is not transferred out of the specimen. The flow stress of PMMA is more temperature sensitive than that of PC, and thus thermal softening is clearly apparent only in the PMMA data. In the high-rate curves, data does not extend past moderate strain levels because of the brittle failure of the split-Hopkinson bar specimens.

The yield stress of PMMA over all of the tested strain rates is documented in Fig. 13. In this case, the material transition seems to occur entirely within the strain rate regime accessed in quasi-static testing,

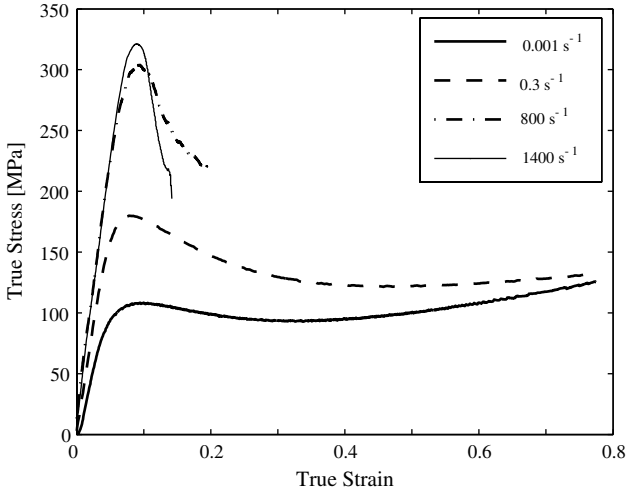

Fig. 12. Representative curves of PMMA true stress–true strain behavior in uniaxial compression at four low, moderate, and high rates. Reported high strain rates are averages over the duration of the tests.

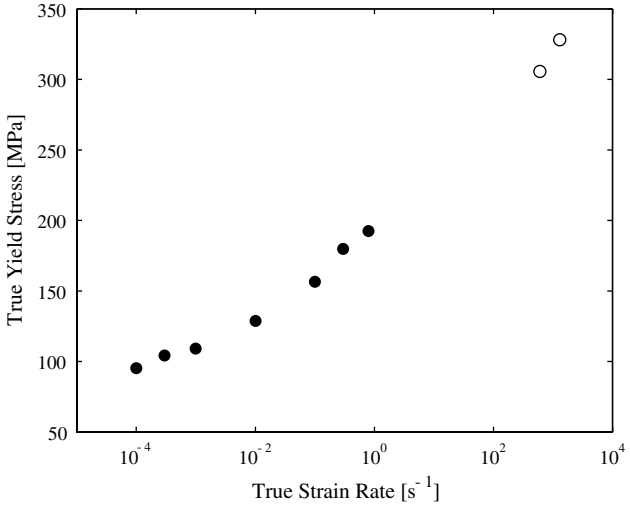

Fig. 13. PMMA true yield stress as a function of true strain rate (logarithmic scale)—low to high strain rates. Each data point represents an average of at least two tests on either the servo-hydraulic Instron (●) or the compressive split-Hopkinson bar (○).

where the yield stress is found to increase in a non-linear fashion with the logarithm of strain rate. This result is consistent with the work of Bauwens-Crowet and Homès (1964) and Roetling (1965b). Though the DSR model for PMMA predicted a material transition, related to the restriction of β-motions, at a strain rate between 10^{-5} s^{-1} and 10^{-4} s^{-1}, Fig. 13 shows a kink in the yield data close to 10^{-2} s^{-1}. However, as with PC, yield data could not be obtained close to the predicted transition region. It is possible that the yield curve begins to deviate from linearity at 10^{-5} s^{-1} to 10^{-4} s^{-1}, but changes only become pronounced at strain rates three to four decades higher. Such a finding would be consistent with the distributed nature of the viscoelastic β-transition observed in the PMMA loss modulus data of Fig. 3; in this figure, the β-peak at a strain rate of $\sim 10^{-3}$ s^{-1} is observed to span two hundred and fifty degrees in temperature.

The experimental yield data presented here, especially in the case of PC, validates the DSR method as an analytical technique for predicting transitions in the rate-dependent behavior of amorphous polymers. With this tool, it will be possible to evaluate different polymers as potential materials for high-rate applications, based on a desire to exploit changes in material behavior. Also, the combined analytical and experimental results presented thus far serve to reinforce the postulated link between the transition in the yield behavior of amorphous polymers and the rate dependence of the α and β transitions in the viscoelastic behavior. Finally, with new insight and new understanding, this fundamental understanding of the material transitions will be used as the foundation for a proposed constitutive model for the three-dimensional rate-dependent finite strain deformation of amorphous polymers.

4. Constitutive model

The constitutive model proposed builds upon prior modeling of the three-dimensional rate-, temperature-, and pressure-dependent finite-strain deformation of thermoplastic materials. The original model was introduced in its components by Boyce et al. (1988) and Arruda and Boyce (1993a,b). The model has been shown to be predictive of the stress–strain behavior of PC (Arruda and Boyce, 1993a; Boyce et al., 1994) and PMMA (Boyce et al., 1988; Arruda et al., 1995) at low to moderate strain rates (10^{-3} s^{-1} to 1 s^{-1}), at temperatures from 300 K to 363 K, and in four states of deformation: plane strain compression, simple shear, uniaxial tension, and uniaxial compression. The model had not been tested against high rate or low temperature data. Here, we extend the model to provide predictive capabilities for high rate and low temperature loading.

There are three components in the original model: a linear elastic spring, a viscoplastic dashpot, and a non-linear Langevin spring. The dashpot and elastic spring act in series, with the non-linear spring in parallel to both. Inherent in this model structure is the assumption that the resistance to deformation may be decomposed into two parts: intermolecular resistance to chain-segment rotation (elastic spring and viscoplastic dashpot), and entropic resistance to chain alignment (Langevin spring). In the proposed constitutive model, it is assumed that the intermolecular deformation resistance may be further decomposed into the contributions from multiple rate-activated processes, each associated with a particular molecular-level motion.

As in most practical applications of the Ree–Eyring yield theory, the proposed model only considers the primary (α) process and the most significant secondary process (β). PC and PMMA data indicates that the contributions from other secondary processes are either hidden within the contribution of the β-process, or are non-existent over the range of temperatures and strain rates capable in mechanical testing. The α-process is associated with rotations of the polymer main-chain segments; in the previous model of Boyce et al, the elastic–viscoplastic component was meant to simulate this process only. The proposed model considers a second, β-component to the intermolecular resistance: in the case of PMMA, it is associated with restricted rotations of the ester side-group; in the case of PC, it is restricted rotations of the main-chain phenyl group. The model assumes that the α and β molecular processes are sufficiently de-coupled, so that overall material response may be approximated as the simple superposition of the two.

A one-dimensional rheological depiction of the proposed constitutive model is presented as Fig. 14. In this model, the β-process is given its own elastic–viscoplastic component, in parallel with the existing "α" elastic–viscoplastic component. The two components have unique material parameter definitions, such that their relative contributions vary with temperature and strain rate. At high temperatures and low strain rates, the β-component will be fairly compliant, and most, if not all, intermolecular resistance will be generated in the elastic spring and viscoplastic dashpot of the α-component. At low temperatures and high strain rates, the β-process will become restricted, and the intermolecular resistance will be two-part. The entropic hardening definition remains unchanged from the original model. A fully three-dimensional constitutive model has been built up from this one-dimensional understanding, beginning with the kinematics of finite strain.

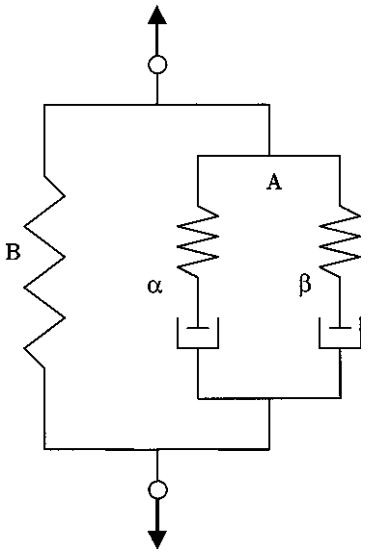

Fig. 14. A one-dimensional rheological interpretation of the proposed constitutive model for rate-dependent thermoplastic behavior.

4.1. Kinematics

The finite strain kinematic framework of the model follows that presented in Bergstrom and Boyce (1998, 2000), Boyce et al. (2000), and Boyce et al. (2001), with the main difference being that every relationship pertaining to the intermolecular resistance is developed in duplicate here. Throughout the derivations of this section, terms relating to the combined elastic–viscoplastic element will be given a subscript of "A", and terms relating to the entropic-hardening element shall be given a subscript of "B" (as denoted in Fig. 14). All quantities specific to the α and β components will be given those subscripts as well. Boldface type indicates tensorial quantities in this three-dimensional formulation.

The total deformation gradient $\mathbf{F} \equiv \partial x/\partial \mathbf{X}$, mapping a material point from the reference position $\mathbf{X}$ to its current location $\boldsymbol{x}$, acts in full on each of the three main components of the model

$$\mathbf{F}_{\mathrm{A}_\alpha} = \mathbf{F}_{\mathrm{A}_\beta} = \mathbf{F}_{\mathrm{B}} = \mathbf{F} \tag{2}$$

The deformation gradients in element A may be multiplicatively decomposed into elastic and plastic components following Kroner–Lee decomposition (Kroner, 1960; Lee, 1969):

$$\mathbf{F}_{\mathrm{A}_\alpha} = \mathbf{F}^{\mathrm{e}}_{\mathrm{A}_\alpha}\mathbf{F}^{\mathrm{p}}_{\mathrm{A}_\alpha} \tag{3}$$

$$\mathbf{F}_{\mathrm{A}_\beta} = \mathbf{F}^{\mathrm{e}}_{\mathrm{A}_\beta}\mathbf{F}^{\mathrm{p}}_{\mathrm{A}_\beta} \tag{4}$$

The plastic deformation gradients $\mathbf{F}^{\mathrm{p}}_{\mathrm{A}_\alpha}$ and $\mathbf{F}^{\mathrm{p}}_{\mathrm{A}_\beta}$ may be interpreted as the mapping of a material point in the reference configuration to a material point in the "relaxed configuration", obtained by elastic unloading to a stress-free state. Also, it is assumed that all plastic deformation is volume preserving, i.e. $\det \mathbf{F}^{\mathrm{p}}_{\mathrm{A}_\alpha} = \det \mathbf{F}^{\mathrm{p}}_{\mathrm{A}_\beta} = 1$. Following polar decomposition of the deformation gradients, the deformation of the relaxed configuration may be expressed as the product of a stretch and a rotation

$$\mathbf{F}^{\mathrm{p}}_{\mathrm{A}_\alpha} = \mathbf{R}^{\mathrm{p}}_{\mathrm{A}_\alpha}\mathbf{U}^{\mathrm{p}}_{\mathrm{A}_\alpha} = \mathbf{V}^{\mathrm{p}}_{\mathrm{A}_\alpha}\mathbf{R}^{\mathrm{p}}_{\mathrm{A}_\alpha} \tag{5}$$

$$\mathbf{F}^{\mathrm{p}}_{\mathrm{A}_\beta} = \mathbf{R}^{\mathrm{p}}_{\mathrm{A}_\beta}\mathbf{U}^{\mathrm{p}}_{\mathrm{A}_\beta} = \mathbf{V}^{\mathrm{p}}_{\mathrm{A}_\beta}\mathbf{R}^{\mathrm{p}}_{\mathrm{A}_\beta} \tag{6}$$

We may examine the rate at which deformation takes place in the body through the velocity gradient $\mathbf{L} = \mathbf{L}_{\mathrm{A}_\alpha} = \mathbf{L}_{\mathrm{A}_\beta} = \dot{\mathbf{F}}_{\mathrm{A}}\mathbf{F}_{\mathrm{A}}^{-1}$. The velocity gradient may be decomposed into elastic and plastic components

$$\mathbf{L}_{\mathrm{A}_\alpha} = \mathbf{L}^{\mathrm{e}}_{\mathrm{A}_\alpha} + \mathbf{F}^{\mathrm{e}}_{\mathrm{A}_\alpha}\mathbf{L}^{\mathrm{p}}_{\mathrm{A}_\alpha}\mathbf{F}^{\mathrm{e}-1}_{\mathrm{A}_\alpha} = \mathbf{L}^{\mathrm{e}}_{\mathrm{A}_\alpha} + \tilde{\mathbf{L}}^{\mathrm{p}}_{\mathrm{A}_\alpha} \tag{7}$$

$$\mathbf{L}_{\mathrm{A}_\beta} = \mathbf{L}^{\mathrm{e}}_{\mathrm{A}_\beta} + \mathbf{F}^{\mathrm{e}}_{\mathrm{A}_\beta}\mathbf{L}^{\mathrm{p}}_{\mathrm{A}_\beta}\mathbf{F}^{\mathrm{e}-1}_{\mathrm{A}_\beta} = \mathbf{L}^{\mathrm{e}}_{\mathrm{A}_\beta} + \tilde{\mathbf{L}}^{\mathrm{p}}_{\mathrm{A}_\beta} \tag{8}$$

where

$$\tilde{\mathbf{L}}^{\mathrm{p}}_{\mathrm{A}_\alpha} = \tilde{\mathbf{D}}^{\mathrm{p}}_{\mathrm{A}_\alpha} + \tilde{\mathbf{W}}^{\mathrm{p}}_{\mathrm{A}_\alpha} \tag{9}$$

$$\tilde{\mathbf{L}}^{\mathrm{p}}_{\mathrm{A}_\beta} = \tilde{\mathbf{D}}^{\mathrm{p}}_{\mathrm{A}_\beta} + \tilde{\mathbf{W}}^{\mathrm{p}}_{\mathrm{A}_\beta} \tag{10}$$

and $\tilde{\mathbf{D}}^{\mathrm{p}}_{\mathrm{A}_\alpha}$ and $\tilde{\mathbf{D}}^{\mathrm{p}}_{\mathrm{A}_\beta}$ (symmetric tensors) represent the rates of plastic stretching in the loaded configuration; similarly, $\tilde{\mathbf{W}}^{\mathrm{p}}_{\mathrm{A}_\alpha}$ and $\tilde{\mathbf{W}}^{\mathrm{p}}_{\mathrm{A}_\beta}$ (skew tensors) are the rates of plastic spin in the loaded configuration. In this analysis, plastic flow is assumed to be irrotational, i.e. $\tilde{\mathbf{W}}^{\mathrm{p}}_{\mathrm{A}_\alpha} = \tilde{\mathbf{W}}^{\mathrm{p}}_{\mathrm{A}_\beta} = \mathbf{0}$. Note that this does not restrict either the elastic or the plastic rotation tensors to be the identity matrix. It follows, then, that

$$\dot{\mathbf{F}}^{\mathrm{p}}_{\mathrm{A}_\alpha} = \mathbf{F}^{\mathrm{e}-1}_{\mathrm{A}_\alpha}\tilde{\mathbf{D}}^{\mathrm{p}}_{\mathrm{A}_\alpha}\mathbf{F}^{\mathrm{e}}_{\mathrm{A}_\alpha}\mathbf{F}^{\mathrm{p}}_{\mathrm{A}_\alpha} = \mathbf{F}^{\mathrm{e}-1}_{\mathrm{A}_\alpha}\tilde{\mathbf{D}}^{\mathrm{p}}_{\mathrm{A}_\alpha}\mathbf{F}_{\mathrm{A}_\alpha} \tag{11}$$

$$\dot{\mathbf{F}}^{\mathrm{p}}_{\mathrm{A}_\beta} = \mathbf{F}^{\mathrm{e}-1}_{\mathrm{A}_\beta}\tilde{\mathbf{D}}^{\mathrm{p}}_{\mathrm{A}_\beta}\mathbf{F}^{\mathrm{e}}_{\mathrm{A}_\beta}\mathbf{F}^{\mathrm{p}}_{\mathrm{A}_\beta} = \mathbf{F}^{\mathrm{e}-1}_{\mathrm{A}_\beta}\tilde{\mathbf{D}}^{\mathrm{p}}_{\mathrm{A}_\beta}\mathbf{F}_{\mathrm{A}_\beta} \tag{12}$$

The final expressions in Eqs. (11) and (12) are integrated to obtain $\mathbf{F}^{\mathrm{p}}_{\mathrm{A}_\alpha}$ and $\mathbf{F}^{\mathrm{p}}_{\mathrm{A}_\beta}$; the elastic portion of the deformation gradients are then obtained via

$$\mathbf{F}^{\mathrm{e}}_{\mathrm{A}_\alpha} = \mathbf{F}_{\mathrm{A}_\alpha}\mathbf{F}^{p-1}_{\mathrm{A}_\alpha} \tag{13}$$

$$\mathbf{F}^{\mathrm{e}}_{\mathrm{A}_\beta} = \mathbf{F}_{\mathrm{A}_\beta}\mathbf{F}^{p-1}_{\mathrm{A}_\beta} \tag{14}$$

The kinematics derived here are general; the material-specific model is defined by the constitutive laws which connect the rates of shape change (plastic stretching) with the stress in the deforming material. Each rate of shape change is given as the product of a magnitude—the plastic strain rate $\dot{\gamma}^{\mathrm{p}}_\alpha$ or $\dot{\gamma}^{\mathrm{p}}_\beta$—and a direction tensor, $\mathbf{N}^{\mathrm{p}}_{\mathrm{A}_\alpha}$ or $\mathbf{N}^{\mathrm{p}}_{\mathrm{A}_\beta}$

$$\tilde{\mathbf{D}}^{\mathrm{p}}_{\mathrm{A}_\alpha} = \dot{\gamma}^{\mathrm{p}}_\alpha\mathbf{N}^{\mathrm{p}}_{\mathrm{A}_\alpha} \tag{15}$$

$$\tilde{\mathbf{D}}^{\mathrm{p}}_{\mathrm{A}_\beta} = \dot{\gamma}^{\mathrm{p}}_\beta\mathbf{N}^{\mathrm{p}}_{\mathrm{A}_\beta} \tag{16}$$

where $\mathbf{N}^{\mathrm{p}}_{\mathrm{A}_\alpha}$ and $\mathbf{N}^{\mathrm{p}}_{\mathrm{A}_\beta}$ are taken to be coaxial with the deviatoric stresses acting on the α and β components of the intermolecular network (A), respectively

$$\mathbf{N}^{\mathrm{p}}_{\mathrm{A}_\alpha} = \frac{\mathbf{T}'_{\mathrm{A}_\alpha}}{|\mathbf{T}'_{\mathrm{A}_\alpha}|} \tag{17}$$

$$\mathbf{N}^{\mathrm{p}}_{\mathrm{A}_\beta} = \frac{\mathbf{T}'_{\mathrm{A}_\beta}}{|\mathbf{T}'_{\mathrm{A}_\beta}|} \tag{18}$$

The material model described here provides constitutive laws for $\dot{\gamma}^{\mathrm{p}}_\alpha$ and $\dot{\gamma}^{\mathrm{p}}_\beta$, as well as the stress tensors $\mathbf{T}_{\mathrm{A}_\alpha}$, $\mathbf{T}_{\mathrm{A}_\beta}$ and $\mathbf{T}_{\mathrm{B}}$.

4.2. Material description

The intermolecular contribution (element A) to the material stress state is related to the deformation by the constitutive laws for the linear elastic springs

$$\mathbf{T}_{\mathrm{A}_\alpha} = \frac{1}{J_\alpha}\mathscr{L}^{\mathrm{e}}_{\alpha}\left[\ln \mathbf{V}^{\mathrm{e}}_{\mathrm{A}_\alpha}\right] \tag{19}$$

$$\mathbf{T}_{\mathrm{A}_\beta} = \frac{1}{J_\beta}\mathscr{L}^{\mathrm{e}}_{\beta}\left[\ln \mathbf{V}^{\mathrm{e}}_{\mathrm{A}_\beta}\right] \tag{20}$$

where $\mathbf{T}_{\mathrm{A}_i}$ ($i = \alpha, \beta$) is the Cauchy (true) stress; $J_i = \det \mathbf{F}^{\mathrm{e}}_{\mathrm{A}_i}$ is the elastic volume change; $\mathscr{L}^{\mathrm{e}}_i$ is the fourth-order modulus tensor; and $\ln \mathbf{V}^{\mathrm{e}}_{\mathrm{A}_i}$ is the Hencky strain. It is assumed that the material is initially isotropic, and that the elastic behavior of the material may be decomposed into α and β components. The modulus tensors may be derived from any two component-specific elastic constants, such as the shear modulus μ and bulk modulus κ

$$\mathscr{L}^{\mathrm{e}}_{\alpha} = 2\mu_\alpha \mathscr{I} + \left(\kappa_\alpha - \frac{2}{3}\mu_\alpha\right)\mathbf{I}\otimes\mathbf{I} \tag{21}$$

$$\mathscr{L}^{\mathrm{e}}_{\beta} = 2\mu_\beta \mathscr{I} + \left(\kappa_\beta - \frac{2}{3}\mu_\beta\right)\mathbf{I}\otimes\mathbf{I} \tag{22}$$

where $\mathscr{I}$ and $\mathbf{I}$ are the fourth-order and second-order identity tensors, respectively. The elastic constants—in this case, μ_i and κ_i ($i = \alpha, \beta$)—are assumed to be *functions of both temperature and strain rate*.[3]

The stress in the non-linear hardening component, the network "back stress" due to the entropic resistance to molecular alignment, is taken to be deviatoric and is defined as in the earlier models using the Arruda-Boyce 8-chain interpretation of molecular alignment

$$\mathbf{T}_{\mathrm{B}} = \frac{C_{\mathrm{R}}}{3}\frac{\sqrt{N}}{\lambda^{\mathrm{p}}_{\mathrm{chain}}}\mathscr{L}^{-1}\left(\frac{\lambda^{\mathrm{p}}_{\mathrm{chain}}}{\sqrt{N}}\right)\overline{\mathbf{B}}'_{\mathrm{B}} \tag{23}$$

where $\lambda^{\mathrm{p}}_{\mathrm{chain}} = \sqrt{\mathrm{trace}(\overline{\mathbf{B}}_{\mathrm{B}})/3}$ is the stretch on a chain in the eight-chain network; $\mathscr{L}$ is the Langevin function defined by $\mathscr{L}(\beta) \equiv \coth\beta - \frac{1}{\beta}$; $\overline{\mathbf{B}}'_{\mathrm{B}}$ is the deviatoric part of the isochoric left Cauchy–Green tensor, $\overline{\mathbf{B}}_{\mathrm{B}} = (\det \mathbf{F})^{-2/3}\mathbf{F}\mathbf{F}^{\mathrm{T}}$; $\sqrt{N}$ is the limiting chain extensibility; and $C_{\mathrm{R}} \equiv nk\theta$ is the rubbery modulus (where n is the number of chains per unit volume, k is Boltzmann's constant, and θ is the absolute temperature). The magnitude of this back stress increases asymptotically as the chain stretch approaches its limiting extensibility.

The total stress in the polymer is given as the tensorial sum of the α and β intermolecular stresses and the network (back) stress

$$\mathbf{T} = \mathbf{T}_{\mathrm{A}_\alpha} + \mathbf{T}_{\mathrm{A}_\beta} + \mathbf{T}_{\mathrm{B}} \tag{24}$$

The effective equivalent shear stresses τ_α and τ_β are given by

$$\tau_\alpha = \sqrt{\frac{1}{2}\mathbf{T}'_{\mathrm{A}_\alpha}\mathbf{T}'_{\mathrm{A}_\alpha}} \tag{25}$$

$$\tau_\beta = \sqrt{\frac{1}{2}\mathbf{T}'_{\mathrm{A}_\beta}\mathbf{T}'_{\mathrm{A}_\beta}} \tag{26}$$

[3] Note that linear viscoelastic theory could be used to capture the relaxation and creep response inherent in these rate-dependent moduli. In the intended applications of this model, however, the rate-dependent finite strain plasticity is the dominating issue of concern and therefore we simply express the elastic properties as functions of strain rate and temperature. Further extension to capture the linear viscoelastic regime of behavior in this rheological element of the model will be addressed in ongoing work.

Finally, two constitutive laws are prescribed for the α and β viscoplastic behavior

$$\dot{\gamma}^{\mathrm{p}}_{\alpha} = \dot{\gamma}^{\mathrm{p}}_{0,\alpha} \exp\left[-\frac{\Delta G_{\alpha}}{k\theta}\left(1 - \frac{\tau_{\alpha}}{s_{\alpha} + \alpha_{\mathrm{p},\alpha} p}\right)\right] \tag{27}$$

$$\dot{\gamma}^{\mathrm{p}}_{\beta} = \dot{\gamma}^{\mathrm{p}}_{0,\beta} \exp\left[-\frac{\Delta G_{\beta}}{k\theta}\left(1 - \frac{\tau_{\beta}}{s_{\beta} + \alpha_{\mathrm{p},\beta} p}\right)\right] \tag{28}$$

where $\dot{\gamma}^{\mathrm{p}}_{0,i}$ ($i = \alpha, \beta$) is the pre-exponential factor proportional to the attempt frequency; ΔG_i is the activation energy; p is the pressure; and $\alpha_{\mathrm{p},i}$ is the pressure coefficient. The internal variable s_i is the athermal shear strength, related to the shear modulus and said to evolve to a preferred state with plastic straining

$$s_{0,\alpha} \equiv \frac{0.077\mu_{\alpha}}{1 - \nu_{\alpha}} \tag{29}$$

$$\dot{s}_{\alpha} = h_{\alpha}\left(1 - \frac{s_{\alpha}}{s_{\mathrm{ss},\alpha}}\right)\dot{\gamma}^{\mathrm{p}}_{\alpha} \tag{30}$$

$$s_{0,\beta} \equiv \frac{0.077\mu_{\beta}}{1 - \nu_{\beta}} \tag{31}$$

$$\dot{s}_{\beta} = h_{\beta}\left(1 - \frac{s_{\beta}}{s_{\mathrm{ss},\beta}}\right)\dot{\gamma}^{\mathrm{p}}_{\beta} \tag{32}$$

where h_i ($i = \alpha, \beta$) is the softening slope and $s_{\mathrm{ss},i}$ is the "preferred state". This internal variable allows the temperature dependence of the yield stress to mimic the temperature dependence of the elastic shear moduli, and its evolution captures the strain softening phenomenon. In the most general form of this constitutive model, the strain softening phenomenon may be considered as the sum of the softening in the α and β components. Overall, Eqs. (27) and (28) capture the rate-, temperature-, and pressure-dependence of yield in the polymer, in addition to strain softening. Further details on the constitutive model proposed here may be found in Mulliken (2004).

4.3. Model implementation

The constitutive model outlined above has been implemented numerically into a commercial finite element code, ABAQUS/Explicit, through a user material subroutine. The application of this user material subroutine requires knowledge of the *16 material constants* that define the components of the model:

Rate-dependent elastic springs		
$\mu_{\alpha}(\theta, \dot{\epsilon})$	$\mu_{\beta}(\theta, \dot{\epsilon})$	Process-specific shear moduli as functions of temperature and strain rate
$\kappa_{\alpha}(\theta, \dot{\epsilon})$	$\kappa_{\beta}(\theta, \dot{\epsilon})$	Process-specific bulk moduli as functions of temperature and strain rate
Viscoplastic dashpots		
$\dot{\gamma}^{\mathrm{p}}_{0,\alpha}$	$\dot{\gamma}^{\mathrm{p}}_{0,\beta}$	Pre-exponential factors
ΔG_{α}	ΔG_{β}	Activation energies
$\alpha_{\mathrm{p},\alpha}$	$\alpha_{\mathrm{p},\beta}$	Pressure coefficients
h_{α}	h_{β}	Softening slopes
$s_{\mathrm{ss},\alpha}$	$s_{\mathrm{ss},\beta}$	Preferred states of athermal shear strengths
Langevin spring		
C_{R}		Rubbery modulus
$\sqrt{N}$		Limiting chain extensibility

Detailed explanation in regards to the determination of these material constants and model parameters is given in Appendix A. It is worth noting here, however, that the reduced DMA data is used directly in the definitions of the elastic springs, and that a piece-wise breakdown of the yield data is used in determining material constants necessary for defining the viscoplasticity.

5. Model vs. experiment

Figs. 15 and 16 demonstrate the ability of the constitutive model to accurately predict the strain rate dependence of PC during uniaxial compression across a broad range of strain rates. Model results and experimental data for the stress–strain behavior at low (10^{-3} s^{-1}), moderate (1 s^{-1}), and high (5050 s^{-1}) strain rates are depicted in Fig. 15. The constitutive model is able to capture the characteristic features of material response to large strain uniaxial deformation: initial linear elasticity, global yield, strain softening, and strain hardening.

The model is shown to capture the rate-dependence of the initial elastic modulus, by incorporating DMA viscoelastic analysis into the formulation. The model does not predict the non-linear transition to yield, as observed in the experimental curves; the model predicts yield as a sudden rather than distributed event. Hasan and Boyce (1995) and, more recently, Anand and Gurtin (2003) have detailed modifications to the model that would enable it to capture this feature of material response. However, for the intended high-rate, large deformation applications of the model, the slight discrepancy is not of concern.

Fig. 16 is a plot of both model and experimental results for PC yield strength over seven decades of strain rate. The plot also shows the model breakdown of the PC yield strength, into α-process and β-process contributions. Even across the transition strain rates, the model predicts the experimental yield strength with less than 5% error. The component-specific yield values indicate that the transition in the overall yield behavior begins when the β-contribution becomes non-negligible. It is clear that the success of the model lies in the decomposition of the intermolecular deformation resistance into the contributions from two distinct molecular processes. The original model, from which this model was derived, only accounted for one molecular process, and thus was only capable of predicting a linear relationship between yield strength and

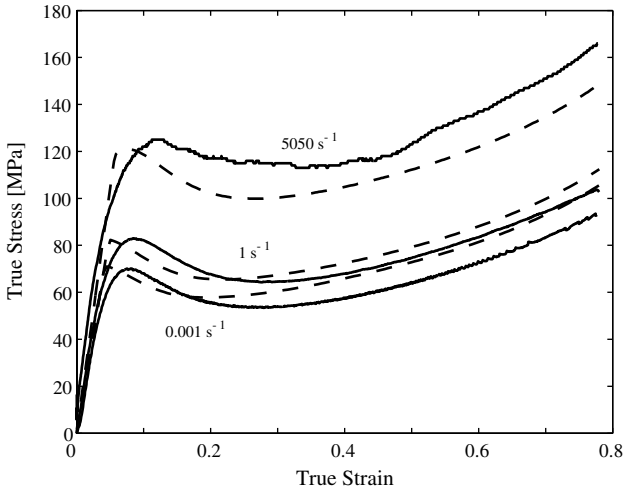

Fig. 15. PC true stress–true strain behavior in uniaxial compression at low, moderate, and high strain rates: model prediction (dashed lines) and experiment (solid lines).

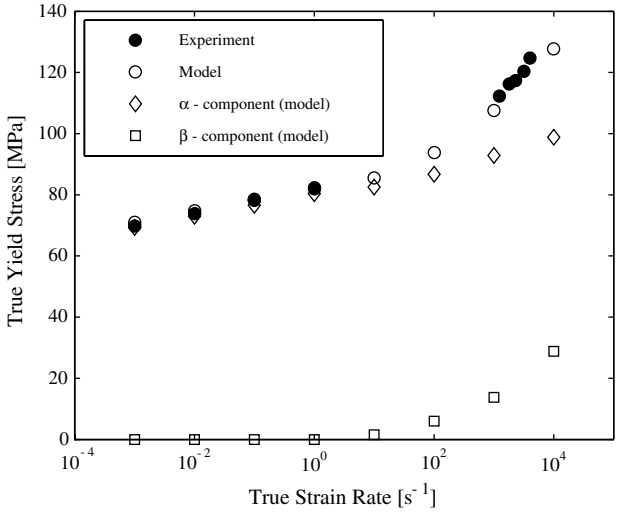

Fig. 16. PC yield behavior in uniaxial compression as a function of strain rate, model prediction and experiment. In addition to the total yield strength, the numerically predicted α and β components of the yield strength are reported, for each strain rate.

the logarithm of strain rate (or near linear, depending on the shear modulus dependence on rate and temperature).

Figs. 17 and 18 provide the same comparison between model and experiment for PMMA as shown in Figs. 15 and 16 for PC. In Fig. 17, the model curves clearly capture the rate-dependence of the initial elastic portion and the yield point of the experimental curves at all strain rates. At the lowest strain rate, the model curve emulates the entire experimental curve up to large strains. However, at moderate and high strain rates, there is a large discrepancy between model and experiment over the post-yield portion of the stress–strain curves. This is due to the significant thermal softening effects that are not accounted for in this

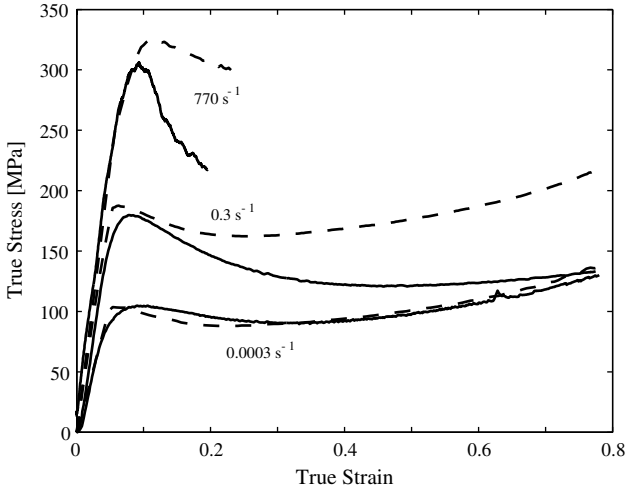

Fig. 17. PMMA true stress–true strain behavior in uniaxial compression at low, moderate, and high strain rates: model prediction (dashed lines) and experiment (solid lines).

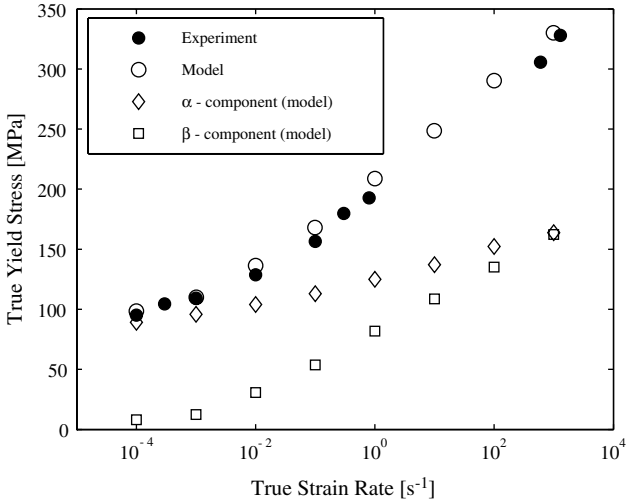

Fig. 18. PMMA yield behavior in uniaxial compression as a function of strain rate, model prediction and experiment. In addition to the total yield strength, the numerically predicted α and β components of the yield strength are reported, for each strain rate.

isothermal constitutive model. In reality, the moderate rate ($10^{-2}\,s^{-1}$ to $10^{-1}\,s^{-1}$) curves correspond to thermomechanically coupled response and the higher strain rate curves correspond to adiabatic deformation. Since the heat generated by plastic work does not have sufficient time to transfer to the surroundings, the temperature-sensitive polymer thermally softens during plastic straining. Recent experiments by Rittel (1999) and Lerch et al. (2003) on PC have indicated that a polymer disk under high-rate ($10^{3}\,s^{-1}$ to $10^{4}\,s^{-1}$) compression may increase in temperature as much as 40 °C with 80% plastic strain. Even at strain rates as low as $10^{-1}\,s^{-1}$, Arruda et al. (1995) observed a 20 °C temperature rise in PMMA disks under large strain compression. This is a critical issue to be addressed in future extensions of the constitutive model, and is a part of current experimental and modeling efforts.

Nonetheless, Fig. 18 demonstrates the ability of this constitutive model to accurately predict the yield strength of PMMA across a very broad range of strain rates. As before, the yield stress breakdown

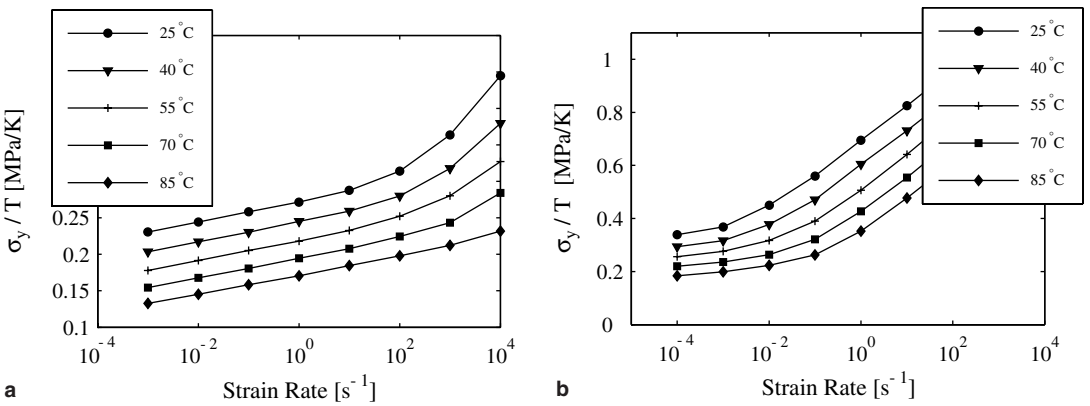

Fig. 19. Model-predicted true yield stress, normalized by temperature, as a function of temperature and strain rate for (a) PC and (b) PMMA.

reinforces the fact that this model's predictive capabilities are built upon a successful decomposition of intermolecular deformation resistance into two separate contributions—α and β.

Fig. 19 provides model predictions of both the PC (a) and PMMA (b) yield strength (normalized by temperature) as a function of strain rate, for a variety of temperatures at and above room temperature. Experimental data for the particular brands of PC and PMMA used in this study has not yet been obtained under all of these conditions, and therefore the quantitative predictions of the model here cannot be verified. However, qualitatively, these two plots demonstrate the general capability of the model in capturing the coupled nature of the rate and temperature dependence of yield. For both materials, the yield transition is predicted to shift to a higher strain rate with increased temperature. This prediction is in accord with the behavior of the β viscoelastic transition, as well as Roetling's experimental yield data (Fig. 1), among others.

6. Concluding remarks

The experimental techniques and corresponding analysis of this study have provided new insight into the rate-dependent behavior of amorphous polymers. Thorough viscoelastic characterization combined with compression testing over a wide range of strain rates has acted to experimentally characterize the influence of material transitions on the rate-dependent behavior of polycarbonate and poly(methyl methacrylate). Both of these materials have been known to exhibit enhanced rate-sensitivity when deformed under high rates of loading, as compared to their behavior under quasi-static rates of loading. This enhanced rate-sensitivity is directly attributable to the restriction of secondary (β) molecular motions. The protocols of this study may be applied to any polymer in order to better understand and predict their mechanical behavior over a wide range of temperatures and strain rates.

In conjunction with the dynamic mechanical analysis (DMA) experiments of this study, new analytical methods were developed in order to translate measured viscoelastic data into a predictive tool that could provide insight into the moderate and high-rate behavior of amorphous polymers. These methods were validated through accurate predictions of the strain rate/temperature conditions of the PC and PMMA yield behavior transitions. By applying the techniques to other amorphous polymers and polymer-based material systems (e.g. polymer nanocomposites), it will be possible to identify, with viscoelastic data alone, those which may offer enhanced properties for impact applications and/or changes in the nature of their rate-sensitivity.

Following the experimental investigation and DMA analysis of PC and PMMA, a new constitutive model for the three-dimensional finite-strain deformation of amorphous polymers was proposed. This proposed model is built upon the transferable framework of an existing continuum-level constitutive model for the rate-, temperature-, and pressure-dependent finite strain deformation of thermoplastics. The model revisions are based on the same concepts which underly both the Ree–Eyring yield theories and the viscoelastic analysis techniques introduced here: intermolecular resistance to deformation may be decomposed into the contributions of different molecular processes, each with their own unique rate and temperature dependence. Though the model introduced here only accounts for the primary (α) and most significant secondary (β) processes, the contributions of other secondary processes (e.g. γ, δ, etc.) could easily be incorporated if material response so dictated.

The proposed constitutive model is shown here to correctly predict yield stress values, as well as the strain rate regime of the transition in the yield behavior, for PC and PMMA. For the case of PC, the model correctly predicts the post-yield stress–strain behavior, up to 0.8 true strain, over the entire range of strain rates tested (10^{-3} s^{-1} to 4000 s^{-1}). However, the isothermal model does not capture the post-yield thermal softening seen in the PMMA stress–strain curves at moderate strain rates. This important aspect of material behavior at moderate and high rates shall be incorporated into future extensions of the model, following a comprehensive investigation of the influence of adiabatic heating and energy storage mechanisms on material deformation resistance. Furthermore, failure mechanisms need to be incorporated into the model

before accurate structural response to impact loading may be simulated. Once these features are in place, however, it will be possible to use model-based FEM simulations to systematically design polymer-based components for high-rate impact applications.

Acknowledgements

This research was supported by the US Army through the Institute for Soldier Nanotechnologies, under Contract DAAD-19-02-D-0002 with the US Army Research Office. The content does not necessarily reflect the position of the Government, and no official endorsement should be inferred. The authors appreciate Dr. Alex A. Hsieh of the Army Research Laboratories for providing the materials used in this study. We also acknowledge Professor S. Socrate and Dr. O. Samudrala for crucial initial design and set-up support of the split-Hopkinson bar facility, as well as the ongoing assistance of Dr. S. Sarva.

Appendix A. Material constants

A.1. Rate-dependent elastic springs

As described in Section 4.2, the material description for the linear elastic springs requires knowledge of any *two* component-specific elastic constants; the values of these constants as a function of both temperature and strain rate must be determined.

The first set of elastic constants and their functional dependence on temperature and strain rate is derived directly from the DMA data. Since the DMA experimentation conducted in this study was performed in uniaxial tension, the elastic storage modulus measured is approximately equivalent to the material's Young's Modulus. By decomposing the measured storage modulus reference curves into α and β components, as described in Section 3.1, we analytically generated component-specific data for the Young's Modulus of the two materials. The component curves give the temperature dependence of these moduli, and the rate-dependent shifts of the corresponding viscoelastic transitions give the strain rate dependence of the moduli. Thus the DMA experimentation and analysis techniques provided here lead directly to half of the material constants needed to describe the linear elastic springs of the model: $E_\alpha(\theta,\dot{\epsilon})$ and $E_\beta(\theta,\dot{\epsilon})$.

Ideally, the values for the second elastic constants would also be derived from rate- and temperature-dependent experimental data. For convenience, it was decided to instead take a second elastic constant as truly constant (in both temperature and strain rate). Of all the elastic constants, the bulk modulus is the least likely to vary significantly with changing temperature or strain rate, even through the material glass transition. However, the question of how to split available bulk modulus values into α and β contributions is not a trivial one. In the end, it was decided to take the Poisson ratio as a constant in both temperature and strain rate, and to give the α and β components the same value of v. For PC, values were set as $v_\alpha = v_\beta = 0.38$; for PMMA, $v_\alpha = v_\beta = 0.35$. It should be noted, however, that once adiabatic heating and thermal softening phenomena are incorporated into the model, it will be very possible for the material to pass through its glass transition with increased plastic straining. At that point, the methods for calculating elastic constants will need revision, for the Poisson ratio of these materials is known to change significantly between the glassy and rubbery regimes.

A.2. Viscoplastic dashpots

Experimental yield data is used to solve for the pre-exponential factors $\dot{\gamma}^{\mathrm{p}}_{0,\alpha}$ and $\dot{\gamma}^{\mathrm{p}}_{0,\beta}$ and the activation energies ΔG_α and ΔG_β. First, the experimentally measured yield values must be decomposed into α and

β contributions, a technique derived from the Ree–Eyring yield models. The component-wise split of the PC yield data is detailed in Fig. A.1. In the case of PMMA, Instron compression tests did not provide yield data close to or below the predicted transition strain rate. Thus, prior to decomposition, the experimental data of this study was supplemented with data generated analytically from the Ree–Eyring model and corresponding α-process parameters given by Bauwens-Crowet (1973).

Following decomposition of the yield data, a pair of simultaneous equations is derived by applying the constitutive law for the rate of plastic straining (Eq. (27) or (28)) to a particular process (α or β) at two different yield points corresponding to two different test strain rates. Appropriate values are substituted in for each of the variables in these equations: the component-specific shear yield values τ are taken from the decomposed experimental yield data; the absolute temperatures θ and the shear strain rates $\dot{\gamma}^{\mathrm{p}}$ are known from the corresponding test conditions, assuming that both processes see the same loading conditions; and the pressures p at yield are determined analytically from the total yield stress and the deformation mode (e.g. uniaxial compression). Also, at yield, the shear strength s has not yet begun to decay—it evolves to a steady state only with plastic straining. Thus the s values at yield may be calculated from Eq. (29) or (31) along with the component-specific elastic constants that correspond to the particular test temperature and strain rate. Finally, assuming that the component-specific pressure coefficients $\alpha_{\mathrm{p},\alpha}$ and $\alpha_{\mathrm{p},\beta}$ are known (discussed later), the only unknown quantities in the two equations are the pre-exponential factor $\dot{\gamma}_0^{\mathrm{p}}$ and the activation energy ΔG_β; these are solved for simultaneously.

In the constitutive equations of the viscoplastic dashpots, there are two other material constants to be specified: the pressure coefficients $\alpha_{\mathrm{p},\alpha}$ and $\alpha_{\mathrm{p},\beta}$. These parameters may be calculated from a quantitative comparison of tension and compression yield data derived from tests at the same temperature and strain rate. Bauwens-Crowet et al. (1972) provide yield data for PC, in both tension and compression, at $4.16\times10^{-3}\,\mathrm{s}^{-1}$ over the temperature range $-125\,^{\circ}\mathrm{C}$ to $125\,^{\circ}\mathrm{C}$. By isolating two regimes in this data—one dominated by the α-process alone, one in which the both the α and β processes are operative—again the yield data may be made component-specific. The component-specific empirical relationships between tensile and compressive yield lead to the PC pressure coefficients $\alpha_{\mathrm{p},\alpha}$ and $\alpha_{\mathrm{p},\beta}$ given in Table A.1.

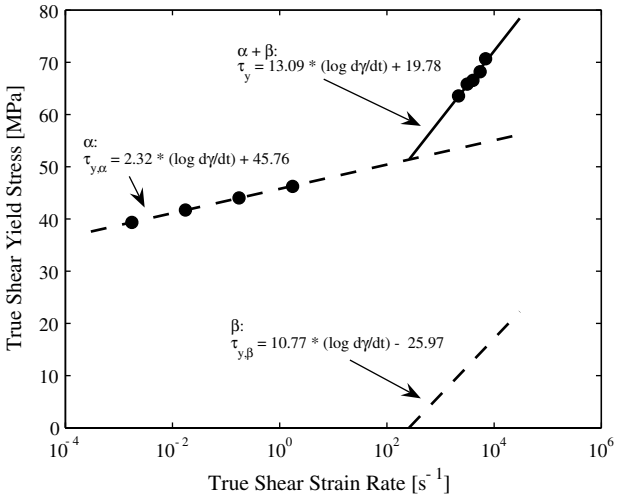

Fig. A.1. Component-wise split of PC true shear yield stress data. Below the transition strain rate ($\sim260\ \mathrm{s}^{-1}$), it is assumed that only the α-process contributes to plastic deformation resistance; above the transition, α and β both contribute. Trendlines fit to the data are used to determine model parameters $\dot{\gamma}_0$ and ΔG.

Table A.1
PC and PMMA viscoplastic model parameters

	PC		PMMA	
	α	β	α	β
$\dot{\gamma}_0^p$ [s^{-1}]	2.94×10^{16}	3.39×10^5	6.95×10^{219}	1.77×10^3
ΔG [J]	3.744×10^{-19}	3.769×10^{-20}	5.528×10^{-18}	6.036×10^{-20}
α_p	.168	.245	.26	.26
h_α [MPa]	250	N/A	200	N/A
$s_{ss,\alpha}$ [MPa]	$0.67 s_{0,\alpha}$	N/A	$0.73 s_{0,\alpha}$	N/A

To determine the pressure coefficients for PMMA, sufficient yield data was not available from any single source in the literature, as had been the case for PC. In fitting the original (single process) constitutive model to experimental PMMA data, Arruda et al. (1995) used a pressure coefficient of 0.26. Based on the strain rates (10^{-3} s^{-1} to 10^{-1} s^{-1}) and temperatures (23–75 °C) of their tests, it may be assumed that this pressure coefficient is an average of the pressure coefficients of the α and β processes. Without any knowledge of the actual breakdown, both the α and β process pressure coefficients were set to 0.26, in order to maintain the average value used by Arruda et al. In future applications of the model, it will be important to obtain more accurate values of these pressures coefficients, perhaps through experimental quantification of the pressure-dependent shift of the α and β transitions.

For both PC and PMMA, the β-process pressure coefficient $\alpha_{p,\beta}$ is taken to be zero in the case of negative pressures. This modification of the original formulation is based upon an assertion that the secondary molecular motions associated with the β-process are only affected by positive pressures, which reduce their mobility. By setting $\alpha_{p,\beta}$ equal to zero under conditions of negative pressure, we prevent the total β-process shear resistance ($s_\beta + \alpha_{p,\beta} p$) from going to zero or even negative in the case of large negative pressures.

The remaining model parameters for the viscoplastic dashpots are related to the internal shear strengths s_α and s_β. In the most general form of this constitutive model, both of these shear strength values evolve with plastic straining, in order to capture the strain softening phenomenon. Four parameters are required to describe this evolution: the softening slopes h_α and h_β and the preferred states $s_{ss,\alpha}$ and $s_{ss,\beta}$. For this study, strain softening in PC and PMMA was captured with evolution only in s_α; s_β was taken as a constant fraction of μ_β. The parameters h_α and $s_{ss,\alpha}$ were determined by fitting the model to the data. Stress–strain curves generated in single-element simulations of uniaxial compression were compared to experimental stress–strain curves. Values for h_α and $s_{ss,\alpha}$ were iterated in parallel in order to achieve optimal agreement between the simulated and experimental stress–strain curves, over the region dominated by strain softening. The strain rates chosen for curve fitting were the lowest ones available, in order to avoid any thermal softening in the data associated with adiabatic heating. The PC and PMMA model parameters h_α and $s_{ss,\alpha}$, determined by curve fitting, are given in Table A.1.

A.3. Langevin spring

The Langevin spring behavior is described by two material parameters: the rubbery modulus C_R and the limiting chain extensibility $\sqrt{N}$. These parameters were determined by fitting model simulations to the

Table A.2
PC and PMMA Langevin spring model parameters

	PC	PMMA
C_R [MPa]	14.2	14.0
$\sqrt{N}$ [$\sqrt{\text{m}}$]	2.3	2.2

By curve fitting are given in Table A.1.

stress–strain data, over the region dominated by strain hardening. Again, the strain rates chosen for curve fitting were the lowest ones available, in order to avoid any thermal softening in the data associated with adiabatic heating. The PC and PMMA model parameters C_R and $\sqrt{N}$, determined by curve fitting, are given in Table A.2.

References

Anand, L., Gurtin, M., 2003. A theory of amorphous solids undergoing large deformations, with application to polymeric glasses. International Journal of Solids and Structures 40, 1465–1487.

Arruda, E., Boyce, M., 1993a. Evolution of plastic anisotropy in amorphous polymers during finite straining. International Journal of Plasticity 9, 697–720.

Arruda, E., Boyce, M., 1993b. A three-dimensional constitutive model of the large stretch behavior of rubber elastic materials. Journal of Mechanics and Physics of Solids 41.

Arruda, E., Boyce, M., Jayachandran, R., 1995. Effects of strain rate, temperature, and thermomechanical coupling on the finite strain deformation of glassy polymers. Mechanics of Materials 19, 193–212.

Bauwens, J., 1972. Relation between the compression yield stress and the mechanical loss peak of bisphenol-A-polycarbonate in the β transition range. Journal of Materials Science 7, 577–584.

Bauwens, J., Bauwens-Crowet, C., Homès, G., 1969. Tensile yield-stress behavior of poly(vinyl chloride) and polycarbonate in the glass transition region. Journal of Polymer Science: Part A-2 7, 1745–1754.

Bauwens-Crowet, C., 1973. The compression yield behavior of polymethyl methacrylate over a wide range of temperatures and strain-rates. Journal of Materials Science 8, 968–979.

Bauwens-Crowet, C., Homès, G., 1964. La dèformation plastique du polymèthacrylate de mèthyle dans le domaine vitreux. Academie des Sciences Comptes Rendus 259, 3434–3436.

Bauwens-Crowet, C., Bauwens, J., Homès, G., 1969. Tensile yield-stress behavior of glassy polymers. Journal of Polymer Science: Part A-2 7, 735–742.

Bauwens-Crowet, C., Bauwens, J., Homès, G., 1972. The temperature dependence of yield of polycarbonate in uniaxial compression and tensile tests. Journal of Materials Science 7, 176–183.

Bergstrom, J., Boyce, M., 1998. Constitutive modeling of the large strain time-dependent behavior of elastomers. Journal of the Mechanics and Physics of Solids 46, 931–954.

Bergstrom, J., Boyce, M., 2000. Large strain time-dependent behavior of filled elastomers. Mechanics of Materials 32, 627–644.

Boyce, M., Parks, D., Argon, A., 1988. Large inelastic deformation of glassy polymers. Part I: Rate dependent constitutive model. Mechanics of Materials 7, 15–33.

Boyce, M., Arruda, E., Jayachandran, R., 1994. The large strain compression, tension, and simple shear of polycarbonate. Polymer Engineering and Science 34, 716–725.

Boyce, M., Socrate, S., Llana, P., 2000. Constitutive model for the finite deformation stress–strain behavior of poly(ethylene terephthalate) above the glass transition. Polymer 41, 2183–2201.

Boyce, M., Kear, K., Socrate, S., Shaw, K., 2001. Deformation of thermoplastic vulcanizates. Journal of the Mechanics and Physics of Solids 49, 1073–1098.

Cady, C., Blumenthal, W., Gray, G., Idar, D., 2003. Determining the constitutive response of polymeric materials as a function of temperature and strain rate. Journal de Physique IV 110, 27–32.

Chen, W., Zhang, B., Forrestal, M., 1999. A split-Hopkinson bar technique for low-impedance materials. Experimental Mechanics 39, 81–85.

Davies, E., 1948. A critical study of the Hopkinson pressure bar. Philosophical Transactions A 240, 375–457.

Davies, E., Hunter, S., 1963. The dynamic compression testing of solids by the method of split Hopkinson pressure bar. Journal of the Mechanics and Physics of Solids 11.

Diaz-Calleja, R., Devine, I., Gargallo, L., Radic, D., 1994. Dielectric-relaxation properties of poly(dimethylphenyl methacrylate)s. Polymer 35, 151–156.

Eyring, H., 1936. Viscosity, plasticity, and diffusion as examples of absolute reaction rates. Journal of Chemical Physics 4, 283–291.

Floudas, G., Higgins, J., Meier, J., Kremer, F., Fischer, E., 1993. Dynamics of bisphenol-A polycarbonate in the glassy and rubbery states as studied by neutron scattering and complementary techniques. Macromolecules 26, 1676–1682.

Foot, J., Truss, R., Ward, I., Duckett, R., 1987. The yield behavior of amorphous polyethylene terephthalate: an activated rate theory approach. Journal of Materials Science 22, 1437–1442.

Gray, G., 2000. Classic split-Hopkinson bar testing. In: ASM Handbook, 12th ed., vol. 8. American Society for Metals, pp. 462–476.

Gray, G., Blumenthal, W., 2000. Split-Hopkinson pressure bar testing of soft materials. In: ASM Handbook, 12th ed., vol. 8. American Society for Metals, pp. 488–496.

Gray, G., Blumenthal, W., Trujillo, C., Carpenter, R., 1997. Influence of temperature and strain rate on the mechanical behavior of Adiprene L-100. Journal de Physique IV 7, 523–528.

Hasan, O., Boyce, M., 1995. A constitutive model for the nonlinear viscoelastic viscoplastic behavior of glassy polymers. Polymer Engineering and Science 35, 331–344.

Haussy, J., Cavrot, J., Escaig, B., Lefebvre, J., 1980. Thermodynamic analysis of the plastic deformation of glassy poly(methyl methacrylate). Journal of Polymer Science: Polymer Physics 18, 311–325.

Hutchinson, J., 1997. The relaxation processes and physical aging. In: Physics of Glassy Polymers, second ed. Chapman and Hall, pp. 128–138.

Kolsky, H., 1949. An investigation into the mechanical properties of materials at very high rates of loading. Proceedings of the Physical Society, B 62, 676–701.

Kroner, E., 1960. Allgemeine kontinuumstheorie der versetzungen und eigenspannungen. Archive for Rational Mechanics and Analysis 4, 273–334.

Lee, E., 1969. Elastic–plastic deformation at finite strains. ASME Journal of Applied Mechanics 36.

Lerch, V., Gary, G., Herve, P., 2003. Thermomechanical properties of polycarbonate under dynamic loading. Journal De Physique IV 110, 159–164.

Moy, P., Weerasooriya, T., Hsieh, A., Chen, W., 2003. Strain rate response of a polycarbonate under uniaxial compression. In: Proceedings of the SEM Conference on Experimental Mechanics.

Mulliken, A., 2004. Low to high strain rate deformation of amorphous polymers: experiments and modeling. Master's thesis, Massachusetts Institute of Technology.

Ree, T., Eyring, H., 1955. Theory for non-Newtonian flow I. Solid plastic system. Journal of Applied Physics 26, 793.

Rietsch, F., Bouette, B., 1990. The compression yield behavior of polycarbonate over a wide range of strain rates and temperatures. European Polymer Journal 10, 1071–1075.

Rittel, D., 1999. On the conversion of plastic work to heat during high strain rate deformation of glassy polymers. Mechanics of Materials 31, 131–139.

Roetling, J., 1965a. Yield stress behavior of poly(ethyl methacrylate) in the glass transition region. Polymer 6, 615–619.

Roetling, J., 1965b. Yield stress behavior of polymethylmethacrylate. Polymer 6, 311–317.

Schartel, B., Wendorff, J., 1995. Dielectric investigations on secondary relaxation of polyacrylates—comparison of low-molecular models and polymeric compounds. Polymer 36, 899–904.

Steer, P., Rietsch, F., 1988. Viscoplasticitè du polycarbonate aux vitesses de sollicitations èlevèes. European Polymer Journal 1, 7–11.

Swallowe, G., Lee, S., 2003. A study of the mechanical properties of PMMA and PS at strain rates of 10^{-4} to 10^{3} over the temperature range 293–363 K. Journal de Physique IV 110, 33–38.

Walley, S., Field, J., 1994. Strain rate sensitivity of polymers in compression from low to high rates. DYMAT Journal 1, 211–227.